

Article

Plasma Electrolysis Spraying Al_2O_3 Coating onto Quartz Fiber Fabric for Enhanced Thermal Conductivity and Stability

Aiming Bu, Yongfu Zhang, Yan Xiang, Yunjie Yang, Weiwei Chen *, Huanwu Cheng and Lu Wang

Department of Materials Science and Engineering, Beijing Institute of Technology, Beijing 100081, China; buaiming@foxmail.com (A.B.); gyshuishangpiao@163.com (Y.Z.); 15624952172@163.com (Y.X.); yyj163email@163.com (Y.Y.); chenghuanwu@bit.edu.cn (H.C.); wanglu@bit.edu.cn (L.W.)

* Correspondence: wwchen@bit.edu.cn; Tel.: +86-10-68912709 (ext. 109)

Received: 23 December 2019; Accepted: 16 January 2020; Published: 19 January 2020



Abstract: This manuscript reported the synthesis of Al_2O_3 coating onto quartz fiber fabric by plasma electrolysis spray for enhanced thermal conductivity and stability. The nano- and micro-sized clusters were partially observed on the coating, while most coating was relatively smooth. It was suggested that the formation of a ceramic coating was followed as the nucleation-growth raw, that is, the formation of the coating clusters was dependent on the fast grow-up partially, implying the inhomogeneous energy distribution in the electrolysis plasma. The deposition of the Al_2O_3 coating increased the tensile strength from 19.2 to 58.1 MPa. The thermal conductivity of the coated quartz fiber was measured to be $1.17 \text{ W m}^{-1} \text{ K}^{-1}$, increased by ~45% compared to the bare fiber. The formation mechanism of the Al_2O_3 coating was preliminarily discussed. The thermally conductive quartz fiber with high thermal stability by plasma electrolysis spray will be widely used in flexible thermal shielding and insulation materials.

Keywords: quartz fiber; Al_2O_3 coating; plasma electrolysis spraying; tensile strength; thermal conductivity

1. Introduction

Quartz fiber has excellent mechanical properties and high thermal stability, light weight, small thermal expansion coefficient [1–6]. It is an ideal structural material to meet the requirements of high performance and light weight. It has become a commonly used material in the aerospace industry after metal alloys. Quartz fiber was not only light in weight, but also has good load-bearing capacity and maintains high stability [7–9]. In recent years, the outstanding mechanical and dielectric properties of quartz fiber have been used in aerospace high temperature radome system, which need high strength and toughness. However, it usually fails under the action of high load.

Therefore, increasing the tensile resistance of quartz fibers performance was of great importance [10–13]. Meanwhile, the demand for high thermal conductivity materials has been increasing. However, metal materials were susceptible to the environment, resulting in decreased performance, lifetime and substantial loss to the production and living [14–16]. In addition, the density of metal materials is too high to be ignored. Therefore, improving the thermal conductivity of quartz fiber is a hot topic of current research. Coating on quartz fibers is considered to be one of the most effective methods to prevent this in the current situation [17–21]. Wang et al. evaluated the filament tensile strength of the bare and PBO-coated quartz fiber before and after 500 °C treated for 30 min. The flexural strength of PBO-coated fiber-reinforced composites is about 50 MPa [22]. Tao et al. studied the tensile strength of the coated quartz fiber fabrics after calcination at 800 °C for 1 h. The tensile

strength of quartz fiber fabric increased gradually with increasing MoSi₂ contents in the coatings [23]. A number of techniques have been deposited in various types coatings onto fiber surface, including chemical vapor deposition, laser ablation, and dip coating. However, these methods have long experimental cycles, and it is still a huge challenge to achieve a uniform thickness coating on the fiber surface [24–26].

We have previously prepared Al₂O₃ coating on the continuous quartz fiber fabric by electrode plasma electrolysis in which the samples were not used as electrodes [27]. Based on the nonelectrode plasma electrolysis, we patented a novel technique, i.e., plasma electrolysis spray, in order to rapidly prepare a coating onto large-scaled fiber fabrics [28]. In the present paper, the plasma electrolysis spray was applied to successfully prepare Al₂O₃ coatings on quartz fiber fabric. In this technology, plasma was generated by cathode, sprayed on the surface of quartz fiber with electrolyte under the action of thermal compression and mechanical compression, and the Al₂O₃ coating was formed by physical and chemical reaction. The tensile properties of the quartz fibers treated for 30 min at 700 °C and then treated for 10 min at 800 °C were studied. The effect of the coating on the high thermal conductivity of quartz fibers was investigated. The formation mechanism of the Al₂O₃ coating was preliminarily discussed [29,30]. We believe that the thermally conductive quartz fiber with high thermal stability by plasma electrolysis spray will be widely used in flexible thermal shielding and insulation materials.

2. Experimental

2.1. Plasma Electrolysis Spraying

Figure 1 shows the schematic diagram of electrolysis plasma spraying Al₂O₃ coating onto the quartz fiber fabric. The anode and the cathode were made of graphite and Cu, respectively. The electrolyte was AlCl₃ aqueous solution with the concentration of 30 g/L. The electrolyte solution was put in from the tail and out from the nozzle of the spray gun. The voltage was gradually applied between the anode and the cathode until a crucial voltage reached 280 V, where a plasma was formed on the surface of the Cu cathode. The plasma was sprayed out of the nozzle under the effect of the flowing electrolyte with pressure, where the pressure was supplied by a high-pressure pump. The electrolysis plasma provided nucleation and growth-up conditions for the Al₂O₃ coating on the quartz fiber fabric. In addition, a large-scaled quartz fiber fabric from Hubei Feilihua Quartz Glass Co., Ltd. and type A plain weave quartz fiber fabric was reasonably coated with the three-dimensional move of the electrolysis plasma spray. In addition, the size of the quartz fiber fabric sample processed in this experiment is 300 × 400 mm. The photo taken during the spray experiment was shown in the inset of Figure 1, where a plasma was obviously observed at the nozzle.

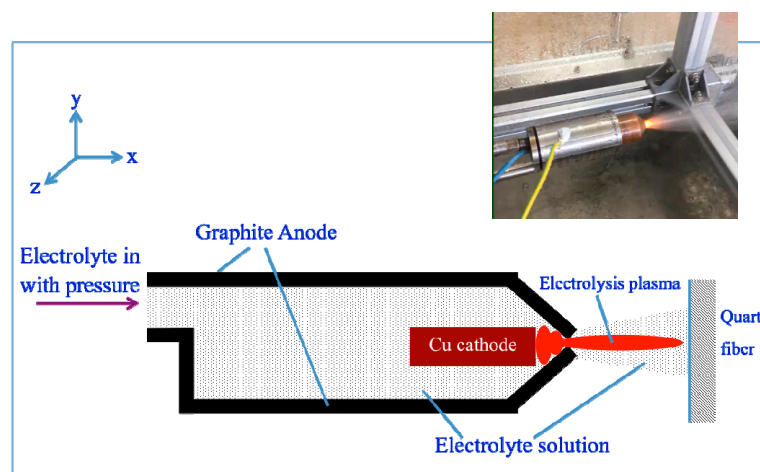


Figure 1. The schematic diagram of the experimental process with the spraying photo shown in the inset.

2.2. Characterization of Coatings

The microstructures of the bare and the coated quartz fibers were characterized by a scanning electron microscope (SEM, S4800, Hitachi, Tokyo, Japan) and an atomic force microscope (AFM, Bruker Multimode 8). The content of the element in the coating was identified by an energy disperse spectroscope (EDS, S4800, Hitachi). The distribution of the element in the coating was characterized by the EDS mapping mode. The chemical structure of the coating was identified by X-ray photoelectron spectroscopy (XPS, PHI Quantera-II, Tokyo, Japan) and Fourier transform infrared spectroscopy (FTIR, FTIR-8400S_IR-21). All tests are performed at room temperature.

2.3. Measurement for Properties

The thermal conductivity was measured by LFA467 Laser Thermal Conductivity Meter at room temperature. In order to precisely measure the thermal conductivity along the longitudinal direction, the fiber bundle was tied into a cylinder with a diameter of 10 mm and then cut into a thickness of 3 mm. Each sample was measured five times in order to obtain the average value. In order to characterize the thermal stability of the quartz fiber, the tensile strength of the quartz fiber was measured after annealing at 700 °C for 30 min and 800 °C for 10 min. The tensile strength was measured by the WDW-E100D Electronic universal testing machine at room temperature. The sample size according to GB type is $\pi(22 \times 2 \text{ cm})$.

3. Results and Discussion

3.1. Surface Morphologies

Figure 2 shows the surface microstructure of the coating on the quartz fiber. The bare quartz fiber was also characterized for comparison purpose. It is shown from Figure 2a that the bare fiber has a typically smooth surface. The deposition of the coating obviously changed the surface, evidenced by the formation of large amounts of clusters on the surface (Figure 2b). The nano- and micro-sized clusters were partially observed, while most coating was relatively smooth (Figure 2b). It was suggested that the formation of a ceramic coating was followed as the nucleation-growth raw, that is, the formation of the coating clusters was dependent on the fast grow-up partially, implying the inhomogeneous energy distribution in the electrolysis plasma.

Three elements, i.e., Si, O, and Al, existed on the surface of the coated quartz fiber, detected by the EDS result in Figure 2d. Both Si and O were also detected on the fiber substrate (Figure 2c). Obviously, the coating was so thin that the element in the substrate was able to be detected by EDS. In addition, Al was confirmed to result from the coating, with the content up to ~11 wt%. The atom ratio between Si and O was calculated to be 1:1.76 for the coated fiber, compared to 1:1.16 for the bare fiber (Figure 2d). Obviously, the deposition of the coating led to the increase of the O content in the EDS result. Undoubtedly the increased O mainly resulted from the coating, revealing that the coating was mainly composed of Al and O. The distribution of Al and O was relatively uniform in the coating, evidenced by the EDS mapping result in Figure 2e.

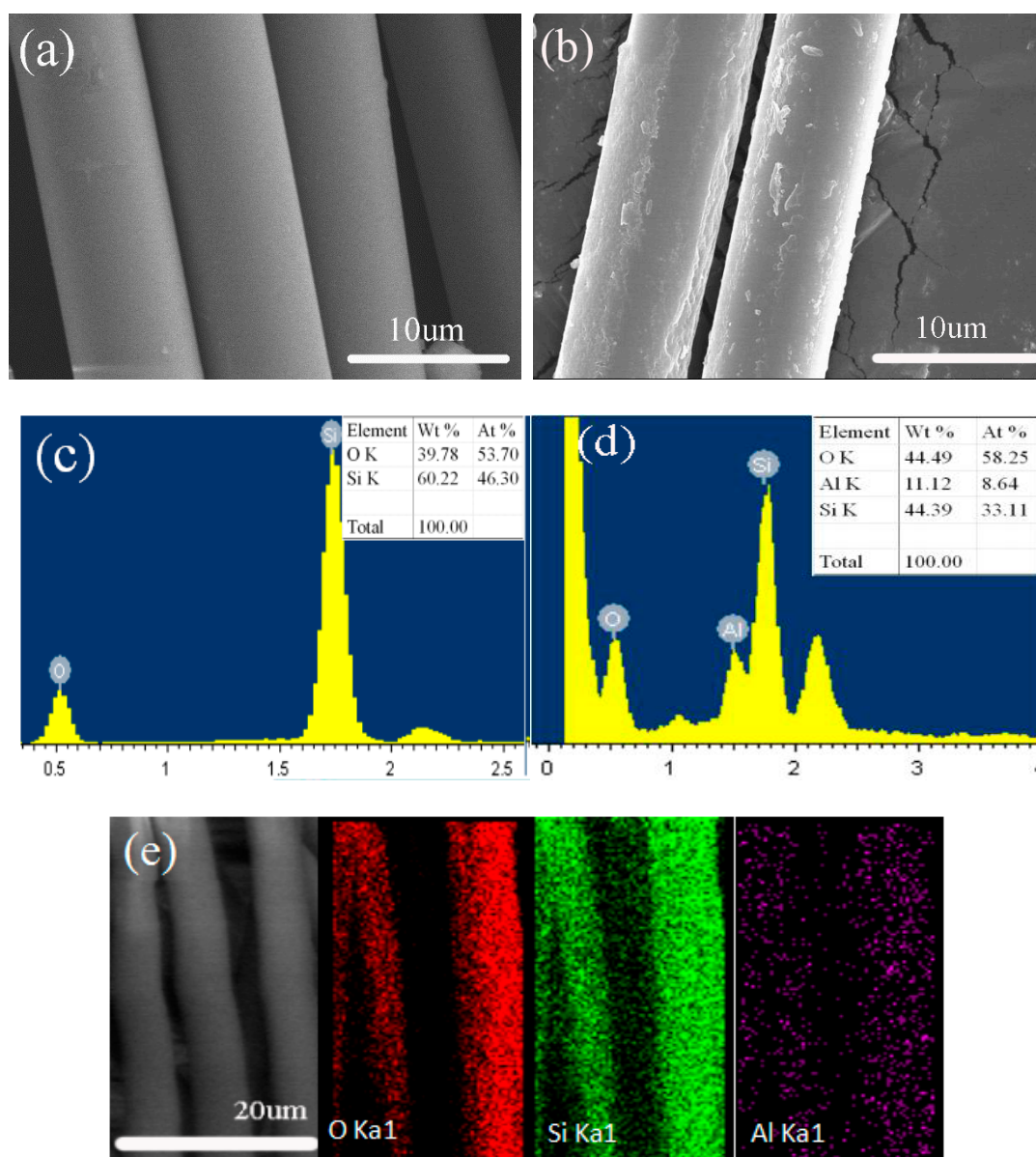


Figure 2. SEM morphologies (a,b), energy dispersive spectroscopy spectra (c,d) and mapping results (e) of the bare (a,c) and coated quartz fibers (b,d,e).

3.2. XPS and AFM Characterization

The chemical structure of the coating was identified by FTIR and XPS, as shown in Figure 3. The peak position at 780 cm^{-1} was caused by the stretching vibration of Al–O–Al, while the peak of Si–O–Si was located at 1086 cm^{-1} (Figure 3a). Figure 3b shows the XPS result of the uncoated and coated fiber. According to different photoelectron binding energy corresponding peak positions, Al 2p, Si 2p, Al 2s, Si 2s, C 1s, N 1s, O 1s were detected to be present for the coated quartz fiber (Figure 3b). The characteristic binding energy of 73.7 eV corresponded to –Al–O– bond (Figure 3b), consistent with the FTIR result in Figure 3a. Both FTIR and XPS results evidenced the characteristic peak of –Al–O–, corresponding to Al_2O_3 , consistent with the EDS analysis in Figure 2c,d.

The fine microstructure of the Al_2O_3 coating was further characterized by AFM, as shown in Figure 4. A relatively smooth surface was observed on the bare quartz fiber (Figure 4a,b), while the deposition of the Al_2O_3 coating increased the surface roughness, evidenced by the formation of the nano-sized Al_2O_3 nodules as shown in Figure 4c,d. After the Al_2O_3 coating was deposited onto the

surface of the quartz fiber, the root-meansquared roughness of the coated carbon fiber increased from 68 to 136 nm. Therefore, the coating is beneficial to improve the surface roughness of the quartz fiber, and enhance the mechanical interlocking and interface adhesion between the fiber and the matrix in the composite material.

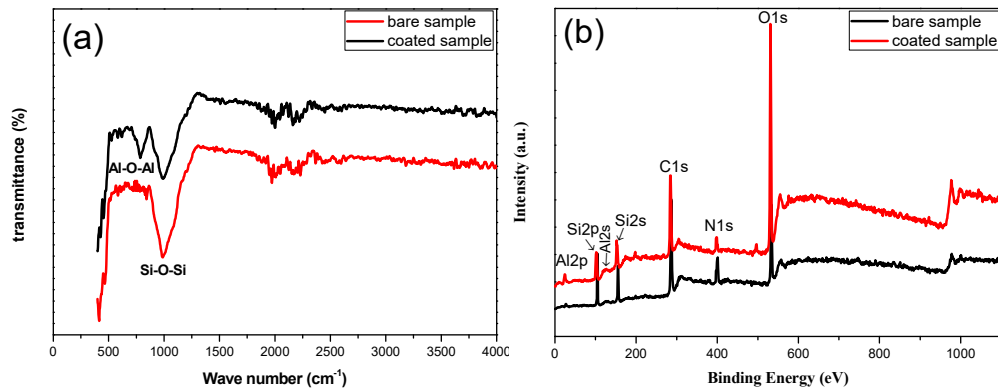


Figure 3. FTIR (a) and XPS (b) spectra of the coated quartz fiber.

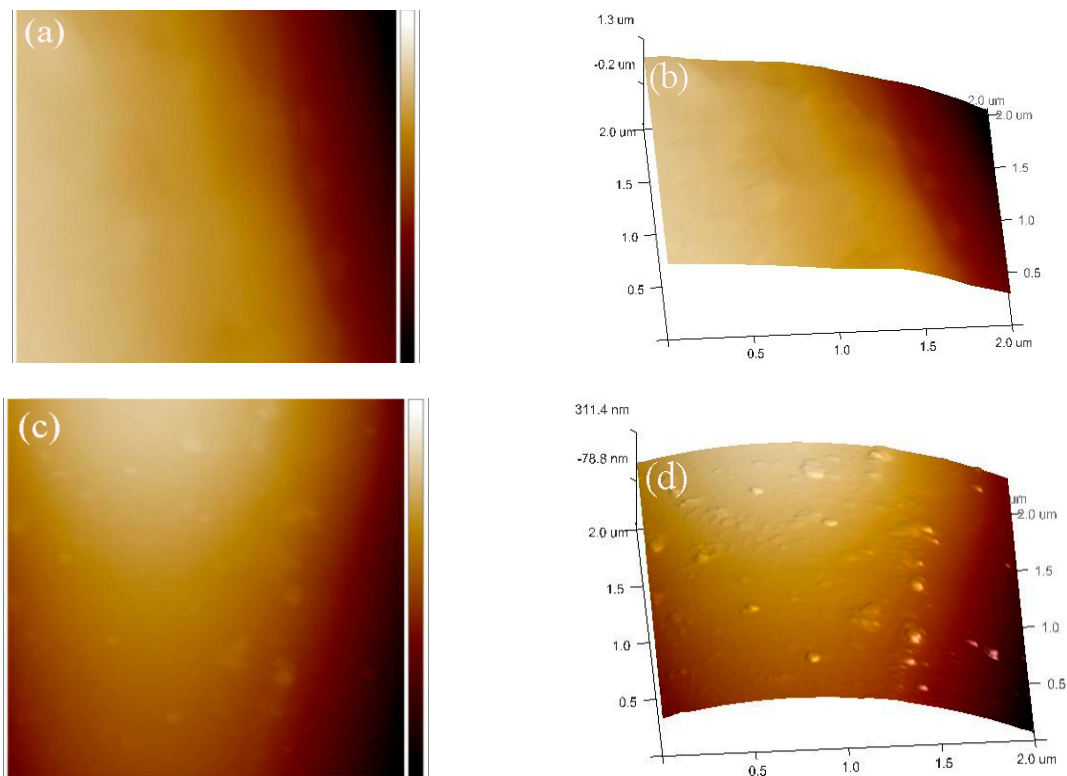


Figure 4. AFM surface topographic images of the bare (a,b) and the coated (c,d) quartz fibers.

3.3. Thermal Conductivity and Stability

Figure 5 shows tensile strength and thermal conductivity of the bare and the coated quartz fibers. The tensile strength of Al_2O_3 -coated quartz fiber was 58.1 MPa, compared to 19.2 MPa of the bare fiber. Obviously, the tensile strength of quartz fiber was greatly improved by the Al_2O_3 coating. The thermal conductivities of coated sample was $1.17 \text{ W m}^{-1} \text{ K}^{-1}$, increased by ~45% compared with the bare sample. The obvious increase of the thermal conductivity mainly resulted from the relatively high conductivity of the Al_2O_3 coating. Meanwhile, the Al_2O_3 coating also protected the quartz fiber at elevated temperatures.

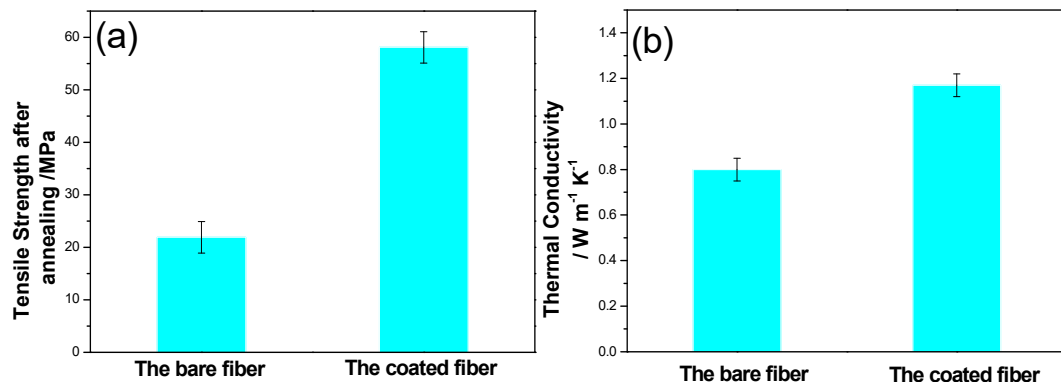


Figure 5. The tensile strength (a) and the thermal conductivity (b) of the bare and the coated quartz fibers.

3.4. Formation Mechanism

Based on the above experimental results, it can be clearly concluded that the plasma electrolysis sprayed Al_2O_3 coating was able to improve the tensile strength and thermal conductivity of the quartz fiber. The formation mechanism of the Al_2O_3 coating has not been fully understood yet. We proposed that the extremely strong potential between the anode and the cathode led to the formation of $\text{Al}(\text{OH})_3$ by AlCl_3 electrolysis, and the $\text{Al}(\text{OH})_3$ gradually evolved into the Al_2O_3 under the thermal effect from the plasma arc.

Figure 6 shows the formation mechanism of the Al_2O_3 coating on the surface of the quartz fiber fabric. When the working voltage was gradually increased, a hydrogen evolution reaction occurs on the surface of the cathode to release a large amount of H_2 . When the working voltage reaches a critical voltage, the breakdown of the vapor envelope causes the plasma to discharge. Electrolyte electrolysis forms a large amount of $\text{Al}(\text{OH})_3$. As the voltage continues to increase, a stable, uniform, continuous plasma arc was formed, along with the electrolyte ejected from the nozzle. After mechanical compression and thermal compression of the plasma arc, $\text{Al}(\text{OH})_3$ dehydrates to form Al_2O_3 on the surface of the quartz fiber. The reactions involved are suggested as follows:

Electrolysis of AlCl_3 and H_2O



Formation of hydroxides



Al_2O_3 formation

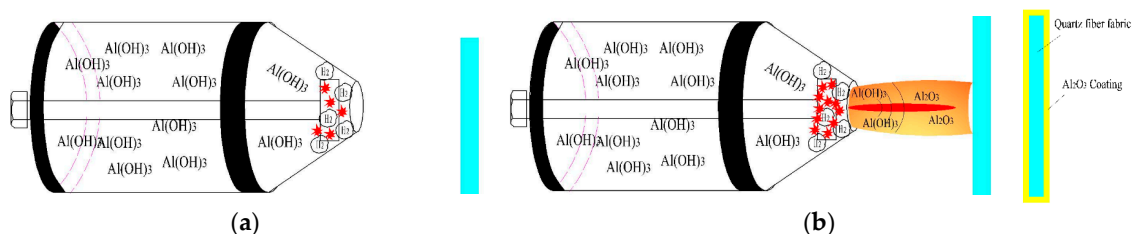


Figure 6. The schematic diagram of the formation mechanism of the Al_2O_3 coating on quartz fiber fabric, (a) H_2 bubble and micro arc formation, (b) stable plasma jet formation, and Al_2O_3 coating deposited on the quartz fiber.

4. Conclusions

A thermally conductive quartz fiber with high thermal stability was achieved by plasma electrolysis spraying. The Al₂O₃ coating was successfully deposited on the quartz fiber with the AlCl₃ aqueous solution. Its tensile properties and high thermal conductivity were studied. The coated sample exhibited very good tensile strength properties after annealing. Compared with the bare sample, the tensile strength increased from 19.2 to 58.1 MPa. The thermal conductivity of the coated quartz fiber also improved due to the high thermal conductivity of the Al₂O₃ coating. The thermal conductivity of coated quartz fiber was 1.17 W m⁻¹ K⁻¹, while the bare sample was 0.81 W m⁻¹ K⁻¹. The formation mechanism of Al₂O₃ coating on quartz fiber surface was preliminarily established.

Author Contributions: Conceptualization, W.C. and L.W.; methodology, W.C. and H.C.; software, A.B. and Y.Z.; validation, A.B. and W.C.; formal analysis, A.B. and Y.X.; investigation, A.B. and Y.Y.; resources, A.B. and Y.Z.; data curation, W.C. and L.W.; writing—original draft preparation, A.B.; writing—review and editing, W.C.; visualization, A.B.; supervision, W.C. and L.W.; project administration, W.C.; funding acquisition, W.C. All authors have read and agreed to the published version of the manuscript.

Funding: This research was funded by the Basic Research Plan, under grant numbers 201720941052 and 201820941208).

Conflicts of Interest: The authors declare no conflict of interest.

References

1. Lu, H.R.; Wang, C.A. Fabrication and characterization of ceramic coatings with alumina–silica sol-incorporated α -alumina powder coated on woven quartz fiber fabrics. *Ceram. Int.* **2013**, *39*, 6041–6050. [[CrossRef](#)]
2. Zheng, Y.; Wang, S. The effect of SiO₂-doped boron nitride multiple coatings on mechanical properties of quartz fibers. *Appl. Surf. Sci.* **2012**, *258*, 2901–2905. [[CrossRef](#)]
3. Kwon, Y.W.; Kim, D.H.; Chu, T. Multi-scale modeling of refractory woven fabric composites. *J. Mater. Sci.* **2006**, *41*, 6647–6654. [[CrossRef](#)]
4. Wang, L.; Huang, Y.D.; Liu, L.; Zhang, J.B. The influence of PBO coating on room temperature mechanic properties of heat-treated quartz fiber-reinforced methyl silicon resin composites I. Flexural properties. *Mater. Sci. Eng. A* **2007**, *465*, 22–28. [[CrossRef](#)]
5. Zheng, Y.; Wang, S.B. Synthesis of boron nitride coatings on quartz fibers: Thickness control and mechanism research. *Appl. Surf. Sci.* **2011**, *257*, 10752–10757. [[CrossRef](#)]
6. Checchetto, R.; Miotello, A.; Guzman, L.; Adami, M.; Chayahara, A. BN coating adhesion on ion-implanted polymer surfaces. *Thin Solid Films* **2001**, *398*, 222–227. [[CrossRef](#)]
7. Arya, S.P.S.; D’Amico, A. Preparation, properties and applications of boron nitride thin films. *Thin Solid Films* **1988**, *157*, 267–278. [[CrossRef](#)]
8. Bai, Z.C.; Chang, M.Y. Controlling fluorescence of a nano-Al₂O₃ film enabled by CdSe quantum dots on CdSe/Al₂O₃ heterojunctions. *J. Lumin.* **2019**, *215*, 116614. [[CrossRef](#)]
9. Zhao, L.; Zhang, L.X.; Tian, X.Y. Interfacial microstructure and mechanical properties of joining electroless nickel plated quartz fibers reinforced silica composite to Invar. *Mater. Des.* **2011**, *32*, 382–387. [[CrossRef](#)]
10. Jiang, Y.G.; Zhang, C.R.; Cao, F. Effects of thermal load on mechanical properties and microstructures of 3D SiO₂f/Si₃N₄-BN composites using polyborosilazane. *Mater. Sci. Eng. A* **2008**, *487*, 597–600. [[CrossRef](#)]
11. Qi, G.; Zhang, C.; Hu, H. Crystallization behavior of three-dimensional silica fiber reinforced silicon nitride composite. *J. Cryst. Growth* **2005**, *284*, 293–296. [[CrossRef](#)]
12. Qi, G.J. TEM investigation on three-dimensional silica fiber reinforced silicon nitride composite. *Adv. Mater. Res.* **2012**, *562*, 431–434. [[CrossRef](#)]
13. Martin, E.; Peters, P.W.M.; Leguillon, J.M.; Quenisset, J.M. Conditions for matrix crack deflection at an interface in ceramic matrix composites. *Mater. Sci. Eng. A* **1998**, *250*, 291–302. [[CrossRef](#)]
14. Carrère, N.; Martin, E.; Lamon, J. The influence of the interphase and associated interfaces on the deflection of matrix cracks in ceramic matrix composites. *Compos. Part A* **2000**, *31*, 1179–1190. [[CrossRef](#)]
15. Zheng, J.; Huang, J.L.; Yang, Q.; Ni, C.Y.; Xie, X.T.; Shi, Y.R. Fabrications of novel solid phase microextraction fiber coatings based on new materials for high enrichment capability. *Trend. Anal. Chem.* **2018**, *108*, 135–153. [[CrossRef](#)]

16. Zheng, Y.; Wang, S.B. Effect of different thickness h-BN coatings on interface shear strength of quartz fiber reinforced Si O C N composite. *Appl. Surf. Sci.* **2014**, *292*, 876–879. [[CrossRef](#)]
17. Qu, M.N.; Yuan, M.J.; He, J. Substrate-versatile approach to multifunctional superamphiphobic coatings with mechanical durable property from quartz sand. *Surf. Coat. Technol.* **2018**, *352*, 191–200. [[CrossRef](#)]
18. Liu, K.; Yao, X.; Jiang, L. Recent developments in bio-inspired special wettability. *Chem. Soc. Rev.* **2010**, *39*, 3240–3255. [[CrossRef](#)]
19. Arukalam, I.O.; Oguziec, E.E.; Li, Y. Nanostructured superhydrophobic polysiloxane coating for high barrier and anticorrosion applications in marine environment. *J. Colloid Interface Sci.* **2018**, *512*, 674–685. [[CrossRef](#)]
20. Zhu, H.; Guo, Z.; Liu, W. Adhesion behaviors on superhydrophobic surfaces. *Chem. Commun.* **2014**, *50*, 3900–3913. [[CrossRef](#)]
21. Baklanova, N.I.; Zima, T.M.; Boronin, A.I.; Kosheev, S.V.; Titov, A.T.; Isaeva, N.V.; Graschenkov, D.V.; Solntsev, S.S. Protective ceramic multilayer coatings for carbon fibers. *Ceram. Int.* **2006**, *201*, 2313–2319. [[CrossRef](#)]
22. Wang, Y.H.; Liu, J.; Wu, X.; Yang, B. Adhesion enhancement of indium tin oxide (ITO) coated quartz optical fibers. *Appl. Surf. Sci.* **2014**, *308*, 341–346. [[CrossRef](#)]
23. Tao, X.; Zhang, L.; Ma, X.H.; Xu, X.J. Preparation of a flexible high emissivity coating on quartz fiber fabric for thermal protection. *Ceram. Int.* **2017**, *43*, 14292–14300. [[CrossRef](#)]
24. Girolamo, G.D.; Blasi, C.L.; Schioppa, M. Microstructural and thermal properties of plasma sprayed mullite coatings. *Ceram. Int.* **2010**, *36*, 1389–1395. [[CrossRef](#)]
25. Xiang, C.S.; Pan, Y.B.; Guo, J.K. Electromagnetic interference shielding effectiveness of multiwalled carbon nanotube reinforced fused silica composites. *Ceram. Int.* **2007**, *33*, 1293–1297. [[CrossRef](#)]
26. Heydt, P.; Luo, C.Y.; Clarke, R. Crystallographic texture and thermal conductivity of zirconia thermal barrier coatings deposited on different substrates. *J. Am. Ceram. Soc.* **2001**, *84*, 1539–1544. [[CrossRef](#)]
27. Xiang, Y.; Zhang, Y.F.; Bu, A.M.; Deng, J.Y.; Meng, Y.; Chen, W.W.; Cheng, H.W.; Wang, L. Preparation, characterization and annealing behavior of nanostructured Al₂O₃ coating on quartz fiber by non-electrode plasma synthesis. *Ceram. Int.* **2019**, *45*, 15520–15525. [[CrossRef](#)]
28. Xiang, Y.; Chen, W.W.; Cheng, H.W.; Bu, A.M.; Zhang, Y.F. Surface Plasma Modification and Coating Properties of Quartz Fiber. *Springer Proc. Phys.* **2019**, *216*, 77–84. [[CrossRef](#)]
29. Zhang, S.G.; Zhang, J.; Jia, R.N.; Lian, Y.; He, Y.D. The effect of electric conductivity on the structure of ceramic coatings prepared by cathode plasma electrolytic deposition. *Mater. Chem. Phys.* **2019**, *224*, 36–39. [[CrossRef](#)]
30. Zhang, Y.P.; Meng, Y.; Shen, Y.H.; Chen, W.W.; Cheng, H.W.; Wang, L. Room-temperature aqueous plasma electrolyzing Al₂O₃ nano-coating on carbon fiber. *Appl. Surf. Sci.* **2017**, *419*, 357–364. [[CrossRef](#)]

